Egyptian Geophysical Society
EGS Journal, Vol. 15, No. 1, 1-18 (2017)

THE IMPACT OF THE SUBSURFACE STRUCTURES ON THE GROUNDWATER OCCURRENCES USING GEOPHYSICAL AND HYDROGEOLOGICAL METHODS IN WADI WL KHARIQ, EL MAGHARA, NORTH SINAI, EGYPT

M.A. Khaled, A.M.M. Al Temamy*, M.S. Barseem*, A.N. El Sayed* and E.A. El Abed***

*Geophysical exploration department, Desert Research Center
**Geology department, Desert Research Center,
1. Matahaf El Matariya street, El Matariya, Cairo, Egypt.

دراسة تأثير التراكيب تحت السطحية على تواجدات المياه الجوفية باستخدام الطرق الجيوفيزيائية والهيدروجيولوجية لوادى الخريق، المغاره، شمال سيناء، مصر

الخلاصـــة: يحتوى وادى الخريق على مساحة شاسعة يمكن استصلاحها. الصخور الكربوناتيه تمثل الخزان الرئيسى للمياه الجوفية. نتائج التفسـير للجسات الكهربية العمودية ادت الى تحديد خمس طبقات جيوكهربية . الطبقة الثالثة و الرابعة والتى تكافىء الحجر الجيرى المتشقق و الحجر الجيرى الطينى تمثل الطبقات الحاملة للمياه الجوفية بمنطقة الدراسة. نتائج التفسير لعدد ثمانية قطاعات جيوكهربية مقطعية ثنائية الأبعاد وضـحت التغيـرات الليثولوجية الجانبية، التراكيب المؤثرة على منطقة الدراسة، توزيع الأنواع المختلفة للحجر الجيرى الحامل للمياه الجوفية و العمق للطبقات الحاملة للمياه. التراكيب المستنتجة من الدراسة الجيوكهربية تمثل بعدد ستة فوالق (F1-F6) . الفالقان F1 و F2 تم استنتاجهما من الجسات الكهربيـة العموديـة و القطاعات الجيوكهربية المقطعية ثنائية الأبعاد. اسطح الفوالق F1, F2, F5 و F6 متصلة بين القطاعات الجيوكهربية المقطعية ثنائية الأبعاد المقاسـة بمنطقة الدراسة. كما بينت القطاعات الجيوكهربية المقطعية ثنائية الأبعاد أن تداخلات الطين مع الحجر الجيرى تزيد فى اتجاه الجزء الشرقى من منطقة الدراسة . نتائج المضاهاه لسجلات اشعة جاما الطبيعية و التكاوين الصخرية للآبار المحفورة بمنطقة الدراسة و كذلك القطاعات الهيدروجيولوجية بينت أن منطقة الدراسة تأثرت بمجموعة من الفوالق (F7-F12) هذه الفوالق تؤثر على تواجد المياه الجوفية و جودتها و أدت الى تكوين تراكيب منخفضة و مرتفعة و كذلك تباين فى السحنات الرسوبية افقيا و تغير فى سمك الطبقات و تواجد طبقة الحجر الجيري المتشقق اسفل الطين المتكلس على أعمـاق مختلفة . معظم الفوالق المستنتجة من هذه الدراسة تأخذ اتجاه شمال غرب-جنوب شرق متفقة مع نتائج التحليل الاتجاهى الكمى و النـوعى للفوالـق و الشقوق بحوض وادى الخريق . يتغذى خزان الحجر الجيرى المتشقق بمنطقة الدراسة عن طريق تخلل المياه السطحية الناتجة عـن سـقوط الأمطـار المحلية على حوض وادى الخريق من خلال التشققات وأسطح الفوالق و اسطح الطبقات بالإضافة الى المياه القديمة للعصور المطيرة السابقة. يتراوح عمق سطح المياه للآبار الحفورة بمنطقة الدراسة بين ٦٠-١١٤ متر من سطح الأرض و ملوحتها تتراوح بين ٢٣٣٥-١٢٣٥٤٨ ملى جرام / لتـر و انتاجية هذه الأبار تتراوح بين ٦٠ -١٢مترمكعب/ساعة والتباين فى إنتاجية الآبار يرجع الى امتداد و تأثير نظم التشققات على الخزان الجوفى.

ABSTRACT: *Wadi El Khariq has a vast area that can be reclaimed. Carbonates represent the main aquifer. The interpretation results of the Vertical Electrical soundings lead to detection of five geoelectrical layers. The third and fourth layers correspond to the fractured and argillaceous limestone, represent the water-bearing layers. The interpretation results of the eight 2-D Electrical Resistivity Tomography (ERT) profiles gave more illustrative information about the lateral facies changes, the structures effect along the study area, distribution of the different types of water-bearing limestone and the depth to these water-bearing layers. The deduced structures from electrical study are represented by the faults F1-F6. The faults F1 and F2 are confirmed from both 1D and 2D imaging profiles. The fault plains of F1, F2, F5 and F6 are continuous between the measured imaging profiles.The 2D imaging profiles revealed that the clay content increase eastwards. The correlation results of the natural gamma and lithological logs of the drilled wells as well as the constructed hydrogeological profiles revealed that the area of study affected by another group of faults (F7-F12). These faults affect on the groundwater occurrence and quality. These faults lead to the formation of graben and horst structures, lateral facies changes, variation in layers thickness and the occurrence of the fractured limestone layer lying beneath the calcareous clay at variable depths. Most of the detected faults in the study area have NW-SE trends coinciding with the lineation analyses of the faults and fractures of El Khariq basin.*

The fractured limestone aquifer in the study area is recharged via the percolation of the surface runoff water of local precipitation on Gable El Maghara catchment area through the fracture lines, fault planes and bedding planes besides paleowater of the paleo-rainy seasons. The depth to water varies from 60 t0 114 m. The groundwater salinity of the wells drilled in El Khariq plain varies greatly due to the effect of the lithological nature of the water-bearing formation and the well design. It varies from 2335 mg/l to 12548 mg/l . The discharge value (Q) varies from 60 m^3/h to 12 m^3/h. This variation is related to the extension and type of the effective fracture systems affecting the concerned aquifer.

INTRODUCTION

The area of wadi El Khariqe basin is located northwest El Maghara area in central Sinai. It has a vast land area suitable for agriculture development in addition to the presence of a good stock of raw coal as a source of energy resources. All of these reasons qualify for establishment of new societies. A research station constructed by the Desert Research Center (DRC) was selected for carrying out this paper as a pilot area in the region. This research station depends on the groundwater produced from a well taping the karast aquifer to irrigate an agricultural experiments and other activities of the manufacturing based crops. The amount of groundwater supply is not sufficient. Therefore, additional some wells is needed to face this demands.

Twenty five % of the world's population used Karst aquifers for drinking water resources and comprise around 40% of the groundwater of United States (Ford and Williams, 2007). While karst aquifers provide important water resources world-wide (e.g., southeastern Appalachian mountains;mid-west USA; Yucatan peninsula; southwestern China; circum-Mediterranean region), they are generally poorly understood due to the spatial and temporal complexity of the flow patterns caused by widely varying porosity and permeability and the organization of the conduit and matrix system. Hydrogeophysics has been a growing field in karst hydrology that has been used in part to improve understanding of distribution of secondary porosity (Jardani et al., 2007; Legchenko et al., 2008; McGrath et al., 2002; Sumanovac and Weisser, 2001; van Schoor, 2002). The highly irregular soil and subsurface bedrock complexity in karst systems has been suggested to limit electrical resistivity tomography (Chalikakis et al., 2011; Thomas and Roth,1999). Dunscomb and Rehwoldt (1999) used 2-D resistivity in a variety of karst terrains with a good deal of success in locating known cave and sinkhole features, as well as confirming suspected fault zones or clay-filled cavities. Faulting may have an effect on ground-water flow paths. The amount of displacement along any particular fault tends to vary, and thus the effectiveness of the fault as a barrier to flow probably changes along the fault plane. Because fault zones can serve as fracture conduits for ground-water flow, characterizing and mapping the structure features in the study area is vital for detecting the suitable sites for drilling wells. Therefore, the present study aims to trace the existed subsurface structures and their impact on the groundwater occurrence and finally to locate the most suitable site for drilling a productive well(s).

The area of study lies in Wadi El Khariq. This wadi is located west Gabel El Maghara and considered as a circular erosion (half circle). Wadi El Khariq area is about 21 km^2 (about5000 Fadden) with a maximum length of about 9 km and maximum width of about 3.4 km. Gabel El Maghara folded belt is one of the famous and large NE – SW folded belt in north Sinai. (fig. 1). The study area is bounded by latitudes 30° 42' and 30° 44' N, and longitudes 33° 18' and 33° 20E.

Climatic condition:

The area of study occupies a portion of the arid belt, which dominates north Egypt and is locally affected by the Mediterranean climate. Sinai was affected by less arid climatic condition (Butzer, 1960). The rainfall is common especially, in the Jan. and Feb. months. The average mean annual rain fall is 103.4 mm/year. The minimum air temperature is recorded during the winter months (October, March, inclusive). The minimum temperature is 5.9°C in March and. The maximum air temperature is 36.2° C in July. The amount of water vapor in the atmosphere is higher in winter than in summer. The annual mean value is 49.6%. Evaporation intensity is generally affected by air temperature, air humidity, wind speed and solar radiation. The mean daily value is about 11.7 mm/day in June. The annual mean is about 4189 mm/year.

In the literature, available information essentially about the hydrogeology of Sinai is limited and is found in the work of Shata et al. (1956), Geofizika company (1963), Hammad (1980), EGSMA (1985, 1986), El Ghazawi (1989), Jica (1992), Yehia (1994) and Hassanein (1997). El Abd (2000).

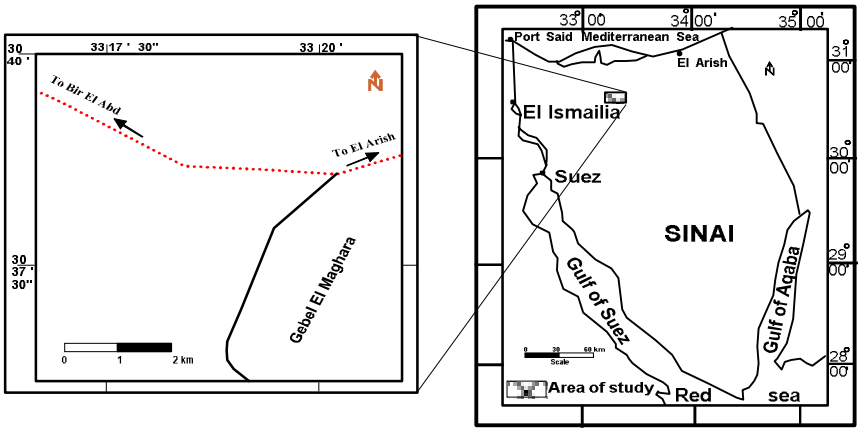

Fig. (1): The location map of the study area hydrGeological studies.

Geomorphological aspect:

The area of study displays morphological features typical of the mild orogenic movements. The existing landforms are affected by strong exogenic processes, which comprise the past wet climatic conditions and the present arid nature of the climate. The main geomorphic units represented such area are classified into the following:

The Structural Ridge:

Gabel El Maghara anticline is one of the strong folds occupied northern Sinai and are arranged “en echelon" in the NE-SW direction (Fig. 2). It dissected into many small folds. It is strongly dissected by fracture lines including both the axial faults and the transversal faults (Fig. 3). Most of such faults determine the orientation of the existing drainage lines.

The Structural Plateau:

This plateau represented by Gabel Mandure synclinal fold (Fig. 2). Its surface is dominantly underlain by hard carbonate rocks belonging to the Upper Cretaceous age. In such plateau the surface is rising to > 500 +MSL.

The Structural Plains:

These structural plains occupy much of the low land areas. They classified into two types. The first type can be termed the inland plains or the intermountain plains and located between the elevated structural features. The second type occupies the down faulted portion and downward area of Gabel El Maghara. Such plain merges to the Mediterranean plain to the northwestern direction.

Geological aspect:

- ***Lithostratigraphy:***

The exposed rocks on Gabel El Maghara range from Jurassic to Quaternary rock units (Fig. 3). In this study we will emphases only on Upper and Middle Jurassic where they represent the main water bearing formations.

The Jurassic rocks are unconformably overlain by Lower Cretaceous sandstone and Upper Cretaceous limestone. The Jurassic rock units are differentiated into three subdivisions which are from base to top (Al Far, 1966).

- Lower Jurassic rock units belong to Mashabba formation at the base, which composed of fluvial sandstone containing large wood fragments with thickness about 100 m. It is succeeded by interbeded shallow marine carbonate and near shore marine Rajabiah (about 248 m) and Shusha (about 271 m) formations.
- Middle Jurassic Rock Units: subdivided into two units. The lower carbonate (Bir El Maghara Formation, 486 m) and the upper clastic (El Safa formation, about 215 m).
- Upper Jurassic (Massaged Formation) Rock Units: dominated by carbonates (about 680 m thick) representing a southerly marine transgression at the end of Bathonian -Callovian times.

- ***The Geologic Structures***

El Maghara Folded Belt is elongate domal features with gentle northwest dip slopes and steep (sometimes vertical and overturned) southeast slopes. It has a length of 45 Km, a width of 20 Km and a maximum relief of 750 m (A.S.L). The folded structure is affected by axial faults (NE-SW), transverse faults (NW-SE) and basalt dikes across it at Wadi El Hamma in the NW-SE direction (Fig. 3).

The middle part of Gabel El Maghara represents the highest part of the structure, which has the form of an asymmetric, east-northeast oriented doubly plunging anticline. The core of this fold is dome-like and exposes 2000 m of Jurassic.

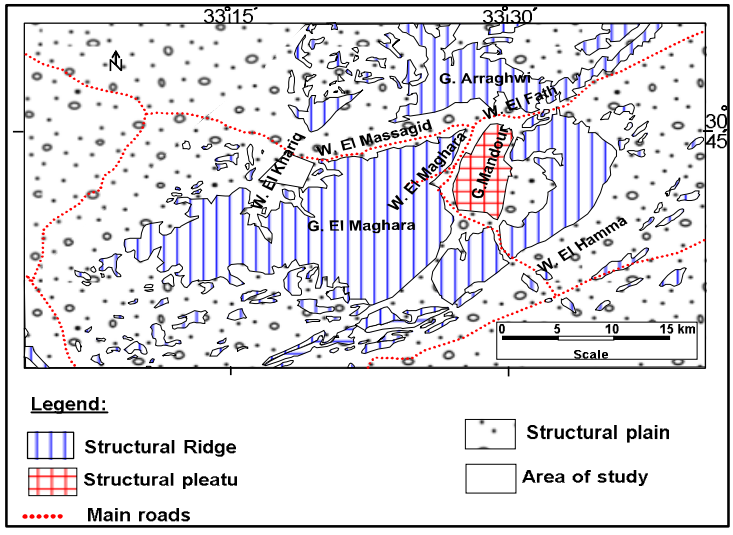

Fig. (2): Geomorphological map Gabel El Maghara.

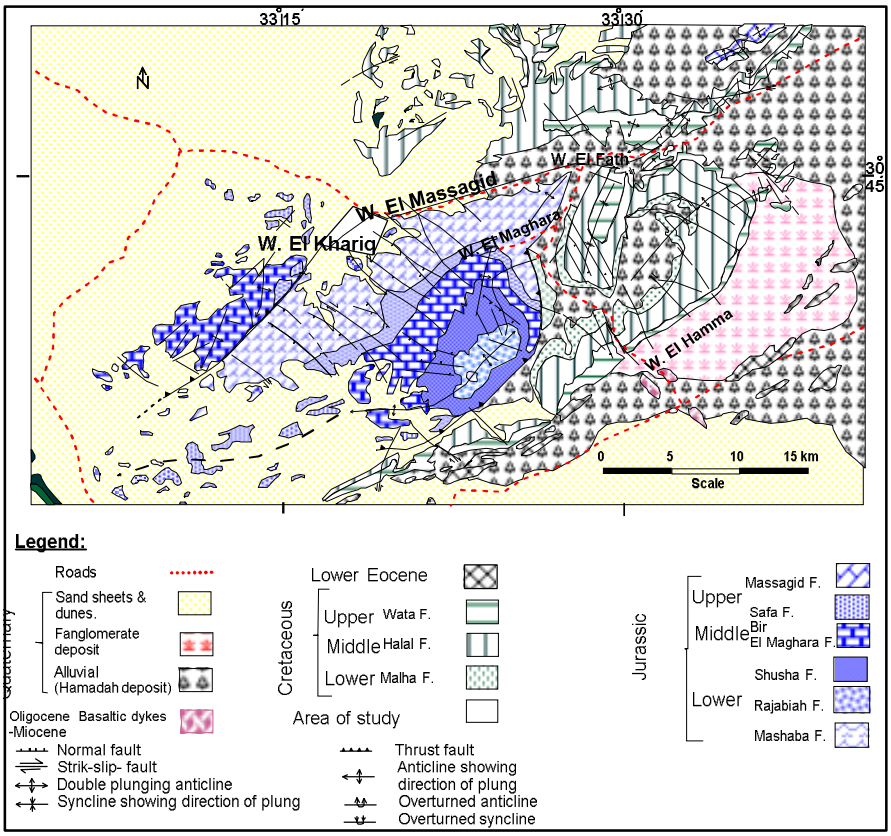

Fig. (3): Geologic map of Gabel El Maghara (After Geological Survey of Egypt (G.S.E.), 1992 - 1994).

Hydrogeological aspect:

The Jurassic aquifers include the Upper and middle Jurassic rocks. Upper Jurassic fissured carbonates dominate Wadi El Massagid and Wadi El Khariq in the northern portion of El Maghara fault-folded ridge. While Middle Jurassic rocks dominate at Wadi El Safa, Wadi El Maghara and Wadi El Malhi.

The Upper Jurassic fractured limestone aquifer (Massagid Formation) is represented by Massagid formation dominating the faulted blocks of the northwestern flank of Gable El Maghara anticline. These strata dip regionally due to northward (average 15°) and constitute the floor of El Massagid plain and the southern cliff of Wadi El Khariq. It overlies El Safa sandstone formation. It is composed of different types of fractured limestone (dolomitic, argillleous, chalky and sandy limestone) intercalated by gypsiferous shale and marl. Its surface is dissected by faults mostly of NE-SW and NW-SE trends (Fig.3). Three wells (FW1, FW2 and FW5) are drilled by Foster Wheeler Italian-Fosweco Division (1990) and tapping this aquifer at wadi El Khariq. The total depths are varies from 153 to 315 m while the depths to water are varies from 98 to 115 m from the ground surface. The rate of production of the three wells vary greatly due to extension and type of effective fractures system affecting on the concerned aquifer beside the lithologic nature of water bearing zones. This is well illustrated in well FW5 (produce 60 m^3/h) where it is drilled along the major fractured zone including the thrust fault between the Middle and Upper Jurassic formations and a set of transverse faults. This structural system facilitates and accelerates the dissolution of limestone to develop favorable karstic features. The lithologic nature of the saturated zone of the water bearing zones is composed of 10 m cavernous limestone 6 m porous sandstone.

Geoelectrical studies:

Electrical resistivity approaches are used extensively in the search for suitable groundwater sources. The ultimate aim of the resistivity survey is to determine the resistivity distribution with depth on the basis of surface measurements of the apparent resistivity and to interpret it in terms of geology or hydrogeology. The geoelectrical investigation plan in the study area revealed the groundwater occurrence, depending on the fractures and secondary porosity of limestone. These fractures mostly associate with the major structures, which may be exposed on the surface or hidden in the subsurface. The more the intensity of the major structures, the more the crowded of the associating fractures. The highly disturbed zones represent the most promising areas for groundwater accumulations. The geoelectrical resistivity survey has been conducted by applying the conventional Vertical Electrical sounding (VES) which measure the apparent resistivity with depth in one dimension (1D) and 2-Dimension Electrical Resistivity Tomography) approaches.

Methodology and Interpretation techniques:

Most of the electrical resistivity techniques require injection of electrical currents into the subsurface via a pair of electrodes planted on the ground. By measuring the resulting variations in electrical potential at other pairs of electrodes, it is possible to determine the variations in resistivity (Dobrin, 1988; Ozcep et al., 2009; Alile et al., 2011). It is necessary to interpret the soundings data taking parameters from other sources like geological and hydrological information into consideration (Kumar et al., 2007, Yilmaz, 2011).

A conventional vertical electrical sounding (VES) survey is used for quantitative interpretation where the center point of the array remains fixed and the electrode spacing is increased for deeper penetration (Loke, 1999). The Schumberger four electrode configuration was used with current electrode half spacing (AB/2) starts from 1m to 2000 m. This electrode separation is sufficient to reach the required depth that fulfils the aim of the study in view of the geologic and hydrogeologic information. Some of these stations were measured near to the existed wells to estimate the geophysical parameters available for verifying the geoelectrical interpretation. Electrical resiuistivity investigation was carried out at five stations in the study areas (Fig. 4) which distributed as grid to cover the study area. Four of them were measured in the corners of the desert research station and the last one at the center.

One of the developments in the resistivity surveying method is the use of two-dimensional (2-D) electrical imaging surveys (Griffiths and Barker, 1993). These techniques are recently widely used in groundwater exploration, environmental and engineering studies because of their ability to detect the variation in resistivity both vertically and horizontally with high resolution (Mahmoud et al., 2015). The theory and applications of this technique were the subject of many geophysical studies (Barker 1996; Osella et al., 1999; Olayinka and Yaramanci, 2000; Schoor, 2002; Marescot and Loke, 2003; and Sumanovac, 2006). They can be used in areas with moderately complex geology where the conventional resistivity sounding method does not give sufficiently accurate results.

The 2-D profiling technique was used for studying the vertical and horizontal variations in electrical conductivity (resistivity) within the study area. The Wenner array, which is an attractive choice for a survey carried out in a noisy area (due to its high signal strength) and also if good vertical resolution is required (Loke, 2001), was used for acquiring the field data, where measurements start at the first traverse with unit electrode separation a = 20 m, and increased at each traverse by one unit, i.e. *2a*, *3a*, *4a*, ….. , *na*; where *n* is a multiplier. The length of the profile, depth of penetration and the required resolution determine the applied unit electrode separation**.** Eight 2D Electrical Resistivity Tomography (ERT) sections were measured in the study area as show in figure (4). The distance between electrodes is 20 m. Each profile has a length of 1420 m. The first and second profiles (P1 and P2) have nearly E-W and NE-SW directions respectively. The other six 2D imaging profiles are measured in NE-SW direction inside the desert research station. Each of the third, fourth and fifth profile was measured through three stages on the same direction by using the roll along property to complete the view of the subsurface layers. The first stage of 2D ERT was measured normally (P3). In the second stage (P4), electrodes of 240m from the southwestern part are transferred forward and the electrodes of 1170 meters are

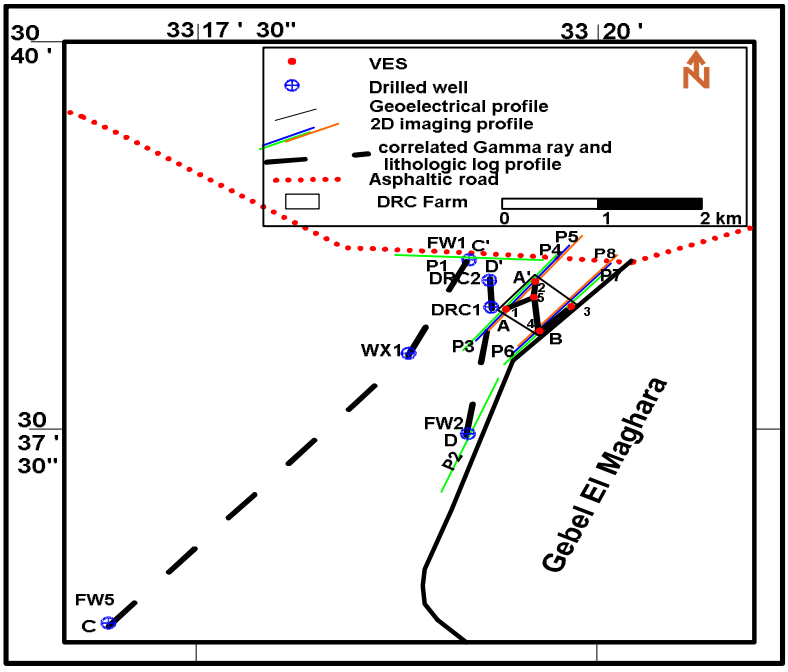

Fig. (4): Geoelectrical field measurements in the study area.

overlapped. Finally, in the third stage (P5) electrodes of 240m from the southwestern part are transferred again forward and the electrodes of 1170 meters are overlapped also. The sixth, seventh and eighth profiles (P6,P7 and P8) are similarly measured parallel to the third, fourth and fifth profiles in NE-SW with the same property of measurements to complete the view of the subsurface layers.

The "Syscal Junior" resistivity meter was used for measuring the resistivity values with high accuracy at different electrode spacing. The topographic survey is carried out to determine the locations (latitudes and longitudes) of the sounding stations on the topographic map and each electrode along different 2D imaging profile by using the GPS apparatus (Trimble type) contact with nine satellites.

The natural Gamma and lithological logs of six drilled wells in the study area (Fig. 4) are correlated through two profiles (C-C' and D-D') to delineate the structure faults affecting the study area and their impact on the groundwater occurrence.

The purpose of the interpretation process is to reach the subsurface setting at the investigated area. The determination of the geoelectrical parameters (the true resistivity and corresponding thickness) for the subsurface layer is a task of the interpretation of geoelectrical data. It includes correlation of these similar or nearly similar parameters in order to illustrate the horizontal continuation and structural configuration. The common features characterizing the lithologies, structural and hydrological settings in the investigated area are described in view of constructed geoelectrical cross sections.

The interpretation of Vertical Electrical Sounding (VES) and 2D imaging profiles are discussed as follow:

I. Vertical Electrical Sounding:

Quantitative Interpretation:

The quantitative interpretation has been done to get a multiple layer model of true resistivities and thicknesses. The true resistivities are related to lithology according to the geologic information of the nearby wells. The computer programs "RESIST" (Van Der Velpen, 1988) and IPI2 (2003)), are used for the quantitative interpretation of the Vertical Electrical Sounding (VES) curves. The available information about the drilled well and the geologic setting of the area is taken into consideration in assigning the lithology to the resulting resistivities. Example of this interpretation was given in figure 5. The interpreted data of each curve represents the geoelectrical layers with their corresponding thicknesses and resistivities. The geologic setting and relevant information are visualized and described in view of a number of generated geoelectrical cross sections crossing the concerned sites in different directions.

2. Two-Dimensional Electrical Imaging (2D):

The resistivity changes along the vertical and lateral directions can be more accurate using the 2D model and the transition from low to high resistivity is quite possible. For the interpretation of the imaging data, the computer program RES2DINV program ver. 3.54 prepared by Loke (1998) was used to interpret the 2-D resistivity imaging measurements. This program determines automatically a 2-D resistivity model for the subsurface for the data obtained from electrical imaging surveys (Griffiths and Barker 1993; Loke 1997).

RESULTS AND DISCUSSION

I. Vertical Electrical Sounding:

The quantitative interpretation of the Vertical Electrical Soundings and the two constructed geoelectrical cross sections A-A' and BA' (figs.6 and 7) revealed that the geoelectrical succession is formed of a number of layers being grouped together in five main layers. The detailed description of the geoelectrical layers from top to bottom is as follows:

The first geoelectric layer represents the surface layer. The resistivity values of this layer range from 6-59 Ohm.m (Table 1). It consists of alluvium deposits mainly from sandy clay and clay.The thickness of this layer varies from 18 m. to 25 m. The second geoelectrical layer consists of dry massive limestone with high resistivity values (161-330 Ohm.m) at VES numbers 1, 2 and 5. The massive limestone layer varies laterally into clay and marl layers at VES numbers 3 and 4. The clay varies in resistivity from 6-8 Ohm.m and in thickness from 48 to 50 m. On the other hand, the marl has a uniform resistivity (15-17 Ohm.m) and a thickness varies from 63m. to 105 m. The variation in lithology of the second layer may due to the lateral facies changes and /or structure effect. The third geoelectrical layer has resistivity values ranging from 58 to 102 Ohm.m. This layer corresponds to water bearing fractured limestone. The thickness of this layer varies from 20 to 40 m. The fourth geoelectrical layer has resistivity values ranging from 30 to 47 Ohm.m. It is equivalent to water bearing argillaceous limestone. The thickness of this layer changes from 35 to 48m. The last detected geoelectrical layer has resistivity values varying from 5 to 18 Ohm.m. This layer consists of clay to marl deposits. The bottom of this layer unreached with the used current electrode separation.

The geoelectrical cross sections illustrate the geoelectrical sequence, lateral and vertical variation of different layers along the profile direction and the subsurface structures affecting the study area. To avoid repetition the following can be concluded:

- The surface alluvium layer (the first geoelectrical layer) is represented at the all cross sections.
- The dry massive limestone (the second geoelectrical layer) changes laterally into clay and marl at VES numbers 3 and 4
- The Water bearing formations in the study area is represented by the fractured limestone (the third geoelectrical layer) and the argillaceous limestone (the fourth geoelectrical layer).

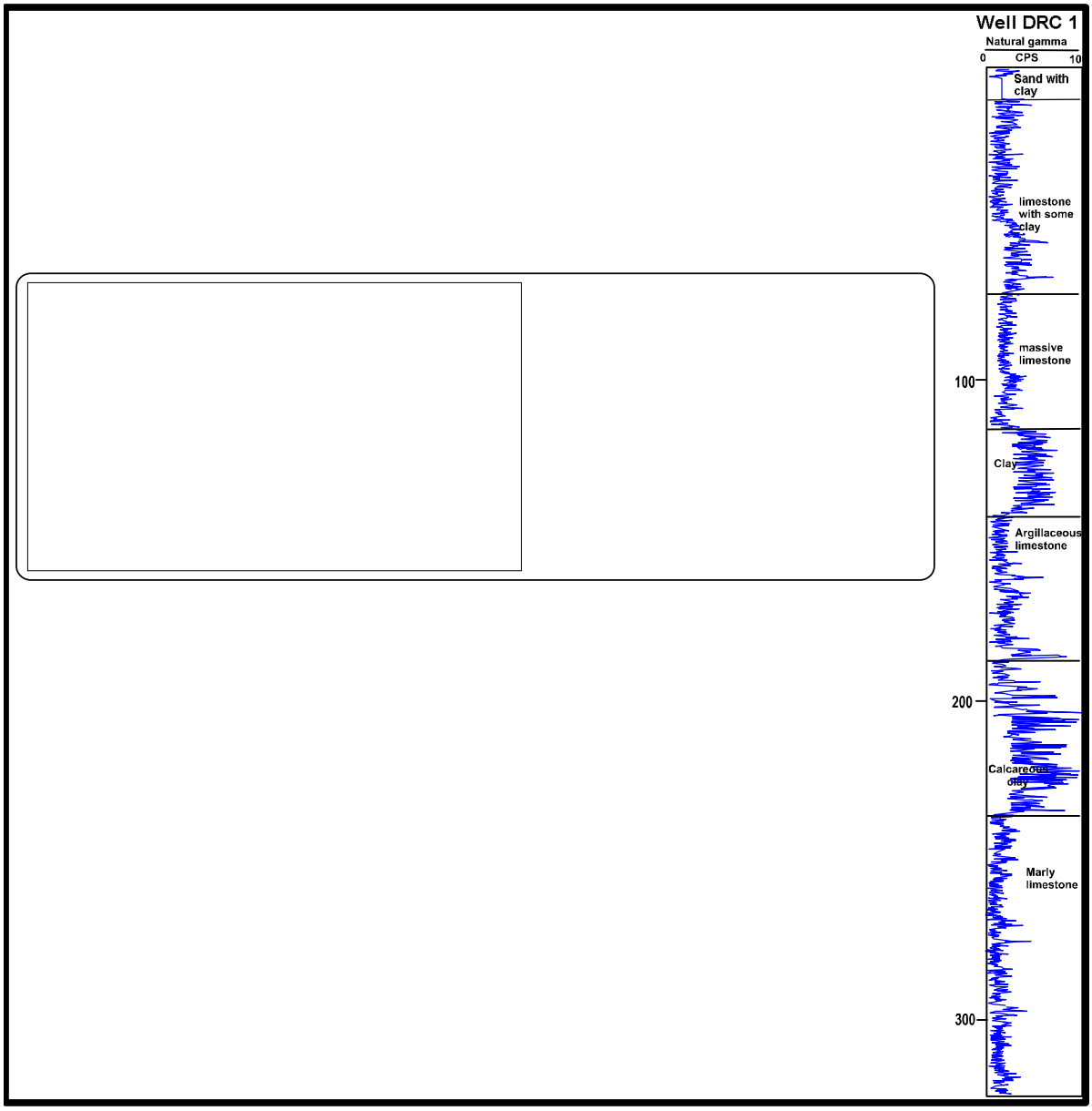

Fig. (5): Interpretation results of VES 1 near to the drilled well DRC1.

Table (1): Resistivities and thicknesses ranges.

Layer	Resistivity (Ohm.m)	Thickness (m.)	Lithology
First layer	6 (VES 2)-52 (VES1)	18 (VES 5)-25 (VES 3)	Alluvium deposits (sandy clay to clay
Second layer	161(VES 2)-330 (VES 5) 6 (VES 3)-8 (VES 4) 15 (VES3) -17 (VES 4)	70 (VES 2)- 133(VES5) 48 (VES 4)-50 (VES3) 63 (VES 4)-105 (VES3)	Dry limestone Clay marl
Third layer	58 (VES 5)-102 (VES 2)	20 (VES 1)-(45 VES2)	Water bearing fractured limestone
Fourth layer	30 (VES 4)-47 (VES 5)	35 (VES 1)-48 (VES 5)	Water bearing argillaceous limestone
Fifth layer	5 (VES 1)-18 (VES 5)	----------	Clay to marl deposits

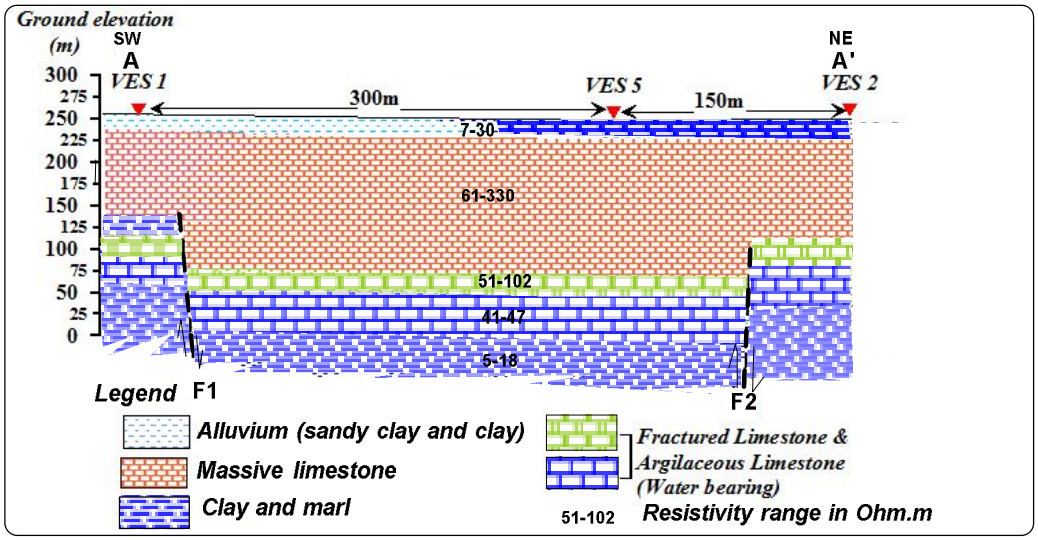

Fig. (6): Geoelectrical cross section AA'.

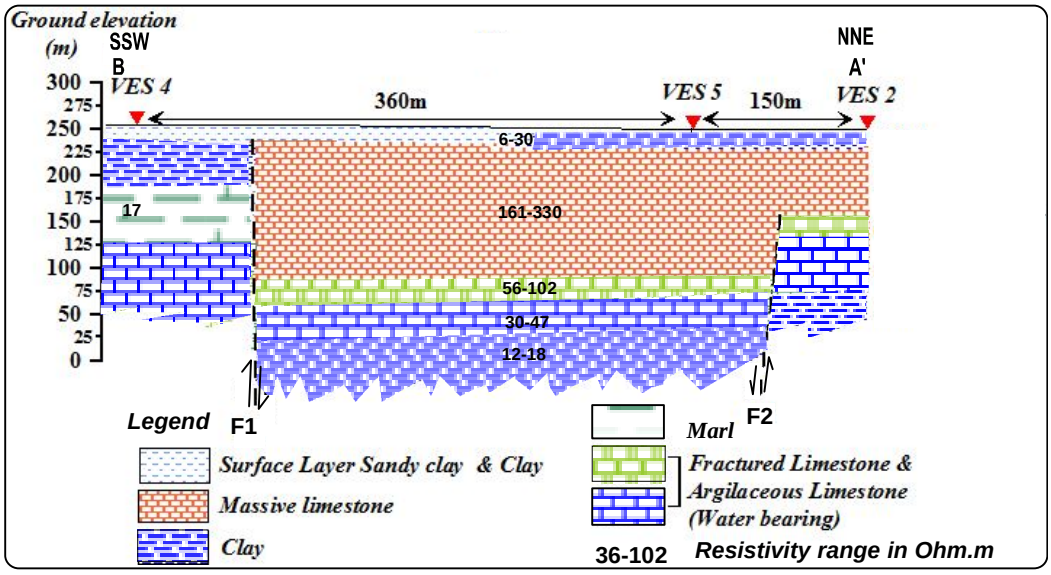

Fig. (7): Geoelectrical cross section BA'.

The water bearing fractured limestone layer (the third geoelectrical layer) was not detected at VES numbers 3 and 4 due to the effect of structures which may be uplifted and eroded or go to downward due to the structure impact.

- The fifth geoelectrical layer is not detected at VES numbers 3 and 4
- Two normal faults (F2 and F3) are detected from the constructed geoelectrical cross sections. The downthrown side of these faults towards the center of the study area and lead to the formation of a basin.

2. Two-Dimensional Electrical Imaging (2D):

The inverted pseudosections are performed using the software RES2DINV program ver. 3.54. The resulting sections display various electrical resistivities ranging from less than 5 Ohm-m to more than 334 Ohm-m (Figures 8-11). Observing the inversion results, the resistivity values have classified into four ranges of resistivities: (5 or less to 16 Ohm-m) represents the conducting clay, (21 to 55 Ohm-m) for the Argillaceous limestone water-bearing, (≥55 to 100 Ohm-m) for the fractured water-bearing limestone and (≥100 to ≥ 334 Ohm-m) for the massive limestone. The inverted section of the first profile (p1) of the E-W direction (Fig.8) generally, shows the presence of vertical structural fault (F3) near the well FW1, with some features. It is observed that, the first conducting layer (5-16 Ohm-m) up to a depth of 40 m in the eastern part of the section meets limestone of different resistivities in the western part. Finally, the easterly massive limestone is underlined by fractured limeston water-bearing. Secondly, the massive limestone underlying the conductive layer that extends to a depth of about 150 m

in the east lies against fractured limestone of less resistivity values in the western part. The depth to water in the well FW1 is 104 m.

The inverted section of the second profile (P2) of the NE-SW direction (Fig.9) generally, shows the presence of a structural fault (F4) south the well FW2, with NW-SE direction. It is observed that, the first conducting layer (5-16 Ohm-m) in the northeastern part of the section meets argillaceous limestone of different resistivities up to a depth of 100 m. This is followed by water-bearing limestone with resistivity ranging from 38 to 100 Ohm-m with a general increase in the southwest wards. This water-bearing layer becomes massive limestone with resistivity more than 100 Ohm-m at the extreme southwestern part.

From the summit inverted sections of the third, fourth and fifth profiles (P3, P4 and P5 (A, B and C respectively)) (Fig.10), it is relevant that, a group of NW-SE faults (F5, F1, F2 and F6) are detected. The argillaceous limestone in the upthrown side of the fault F5 meets conductive clay in the downthrown side. The argillaceous limestone in the upthrown side of the fault F1 contacts massive and fractured limestone in the downthrown side from a depth of 45 m to about 14om. On the other hand, the fairly massive and fractured limestone in the upthrown side of the faults F1 and F6 lie against the massive limestone in the downthrown side up to a depth of 160 m followed by argillaceous limestone in the upthrown side against the fractured limestone in the downthrown side of the fault F6 but the argillaceous limestone dip in the downthrown side of the fault F1.The depth to water in the upthrown side is 120 m whereas in the downthrown side is 165m.

From the second summit inverted sections of the sixth, seventh and eighth profiles (P6, P7 and P8 (A, B and C respectively)), (Fig. 11,), it is relevant that, the same group of NW-SE faults (F5, F1, F2 and F6) are detected indicating that these structures are continuous (Fig. 12). In the second summit inverted sections the argillaceous limestone in the upthrown side of the fault F5 meets conductive clay in the downthrown side. The argillaceous limestone in the upthrown side of the fault F1 contacts the conductive clay in the downthrown side from a depth of 120 m to the end of the section (depth of 240 m.). On the other hand, the argillaceous limestone in the upthrown side of the faults F1 contacts the conductive clay in the downthrown side. The massive limestone followed by argillaceous limestone and conductive clay in the downthrown side of the fault F6 contact argillaceous limestone in the upthrown side. Generally, the expected depth to water in the second summit inverted sections reach nearly to 120 m. This summit has more clay content comparable with the first summit. Therefore, it is expected that the water-bearing limestone in the second summit inverted sections of the sixth, seventh and eighth profiles (P6, P7 and P8) has a higher salinity comparable with the water-bearing limestone in the first summit inverted sections (P3, P4 and P5).

It can be concluded from the 2-D ERT profiles that the area of study is characterized by heterogeneity for resistivity values in vertical and horizontal direction due to the effect of structural faults in the study area. The moderate resistivity values of argillaceous limestone and fractured limestone that varies from 50–100 Ohm.m is the most suitable for drilling exploitable water wells in the study area. The thickness of the water-bearing limestone is variable along the study area.

3- Inferred structures from the correlation of the natural gamma and lithological logs:

To correlate the gamma and lithological logs of the drilled wells in the study area, the marker beds of calcareous clay and clay are used as marker beds in the correlation process. The correlation results of the first profile C-C' (Fig. 13) connecting between the wells of Fw1, Wx1 and Fw5 revealed that the well Wx1 represents a graben like structure between the faults F7 and F8. F7 lies between the wells Fw1 and Wx1. The fault F8 lies between the wells Fw5 and Wx1. The wells Fw5 and Fw1 represent the best wells in the study area. These wells produce from the fractured limestone beneath the calcareous clay. This layer meets clay, argillaceous limestone and calcareous limestone in well Wx1. The upper part of the limestone water bearing is penetrated in the bottom part of well Wx1 so the productivity of this well is very low. Therefore, it is recommended to penetrate the full layer in the location of well Wx1.

The correlation results of the second profile D-D' connecting between the wells of DRC2, DRC1 and Fw2 (Fig.14) revealed that the well DRC1 represent a horst like structure between the two sided wells Fw2 and DRC2 due to the effect of faults F9 and F10. The well DRC2 has the highest salinity well in the study area as this well produces from the argillaceous limestone with high clay content. The upper part of the water bearing limestone lying beneath the calcareous clay in profile C-C' is represented with a small thickness in the lower most part of well DRC2. A larger thickness of this layer is reached in well DRC1. This layer was not reached in well Fw2 where this well is drilled with a small thickness. To enhance the water quality at well DRC2 it is recommended to penetrate the layer beneath the calcareous clay with a large thickness. Therefore, it can be concluded that the fractured limestone layer lying beneath the calcareous clay is found at variable depths in the study area due to the impact of faults affecting the study area.

Groundwater condition:

Karst aquifer is limestone or easily dissolved rock and formed collectively from the unconsolidated cover over the bedrock, narrow fractures in the bedrock, small conduits, and larger cave passages. The conduits and caves consist from the pore space between the limestone grains (intergranular or primary porosity) and the fractures (secondary porosity) formed by joints, bedding planes, and faults.

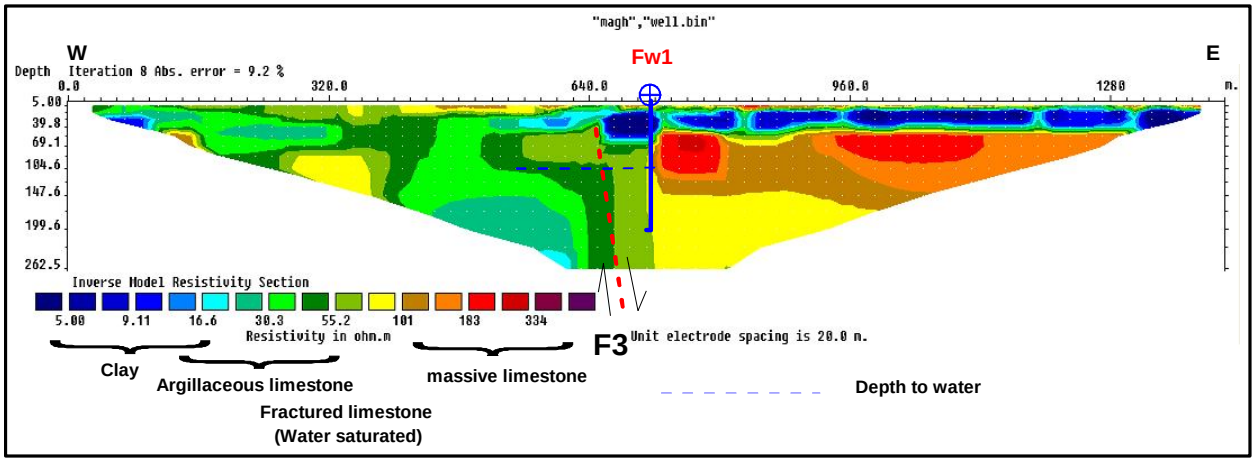

Fig. (8): Inverted resistivity model of 2-D electrical resistivity tomography (2D No.1).

The openings pores may be filled partly or completely by water. The elevation where all pores are filled with water in an aquifer is the water table and it is highly irregular due to the developing of conduits at various elevations. Geophysics can help identify locations for well drilling, investigate subsurface cavities and obtain other information on the aquifer structure.

The fractured limestone aquifer in the study area is recharged by the percolation of the surface runoff water of local precipitation on Gable El Maghara catchment area through the fracture lines, fault planes and bedding planes besides paleowater of the paleo-rainy seasons (El Abd, 2000). The groundwater salinity of the wells drilled in El Khariq plain varies greatly due to the effect of the lithological nature of the water bearing formation and the well design. It varies from 2335 mg/l (Well FW1) to 12548 mg/l (well DRC2). High salinity of (well DRC2) is attributed to high content of gypsiferous shale, marl and argillaceous limestone within the water bearing formation (El Abd and Sadek 2010) and as shown in correlation lithological wells (Fig. 15).

The hydraulic parameters of this limestone aquifer have been determined by RIWR (1984 and 1988), EGSMA (1985 and 1986) 1990 and they found that the transmisivity (T) values vary from $6X10^{-5}$ to $2 X 10^{-2}$ $m^{2/}$sec. The transmisivity (T) values are low reflecting the effect of the lateral facies changes and/or fractures system. The storativity (S) values vary from $4.3X10^{-1}$ to $.5X10^{-3.}$ The discharge value (Q) varies from 60 m^3/h to 12 m^3/h (Table 2). The rates of production of the wells vary greatly due to the extension and type of the effective fracture system affecting the concerned aquifer.

Structural impact on the groundwater occurrence

The Interpretation results of the Vertical Electrical Soundings (VESes) and 2D ERT profiles revealed that the area of study is affected by six faults F1to F6 (Fig.16). The faults F1 and F2 were detected from both VESes and 2D electrical tomography profiles and form a local basin in between. Most of these faults have NW-SE trend with different degree. The faults F1, F4 and F6 have downthrown side northeastward whereas the fault F2 and F5 have downthrown side southwestward. The fault F3 has nearly N-S direction and its downthrown side towards the east direction. it is relevant that, the group of NW-SE faults (F1, F2, F5 and F6) are continuous in the 2D ERT P3, P4 and P5 as well as P6, P7 andP8.

According to the throw of faults, the study area of Desert Research Station is located in basin whereas the clay deposit is concentrate. The structure effect causes the lower geoelectrical layers (limestone) changed into argillaceous limestone and clay eastwards. This affects on the potentiality of water bearing layer due to low permeability and the exploited water from the drilled well become more saline. The structure effect is also reflected on the changeable thickness of these layers. The faults play an important role in existing groundwater whereas the fractures concentrate on the sides of faults that increase according to type of rocks. These fractures act as the best locations for storing the groundwater. The best sites for drilling productive wells with good quality of groundwater will be detected according to the location of faults and the type of rock around it. The first and second priority for drilling water well (Fig.16) are determined beneath the electrode locations of 870 m. and 300 m. respectively at the 2D ERT profile P5 (C in Fig. 10). The deduced structure from both the correlated gamma and lithological logs (Figs.13 and 14) as well as the hydrogeological cross sections (Fig.15) is represented by the faults F7 to F12. Most of these faults have NW-SE trend with different degree (F7, F8 and 12). The fault F7 and F12 have downthrown side southwestwards whereas the fault F8 has downthrown side northeastwards. The faults F9 and F10 have near E-W and WNW-ESE trends respectively. The fault F9 has downthrown side northwards but the fault F10 has downthrown side southwards. The fault F11 has NE-SW trend with downthrown side southeastwards.

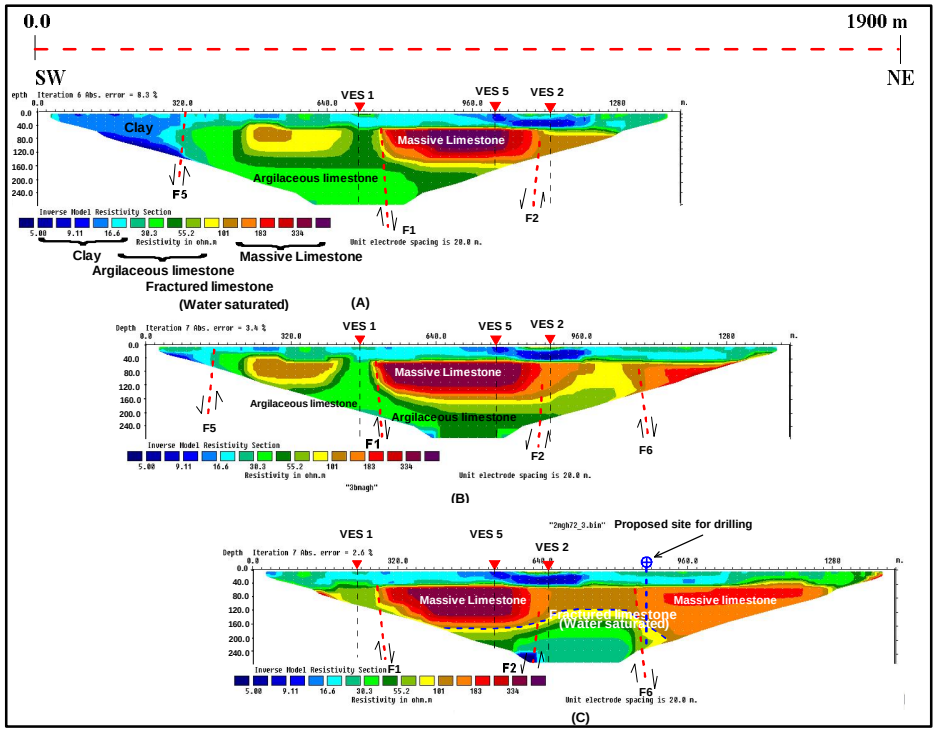

Fig. (10): Inverted resistivity model of the third, fourth and fifth (P3, P4 and P5 (A, B and C respectively)) 2-D electrical resistivity tomography.

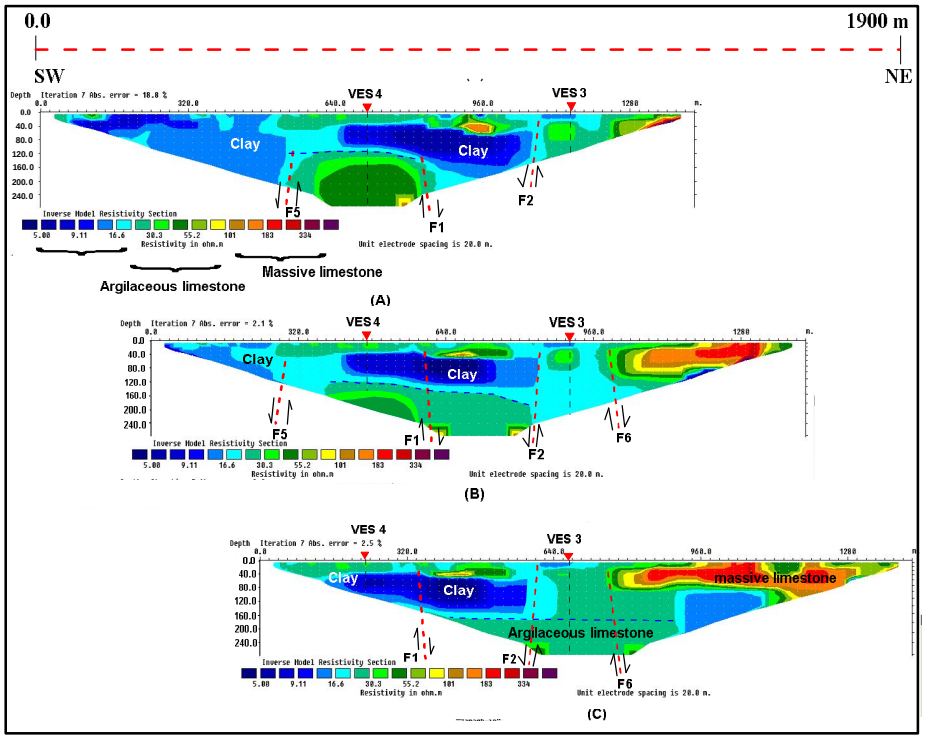

Fig. (11): Inverted resistivity model of the sixth, seventh and eighth (P6, P7 and P8 (A, B and C respectively)) 2-D electrical resistivity tomography.

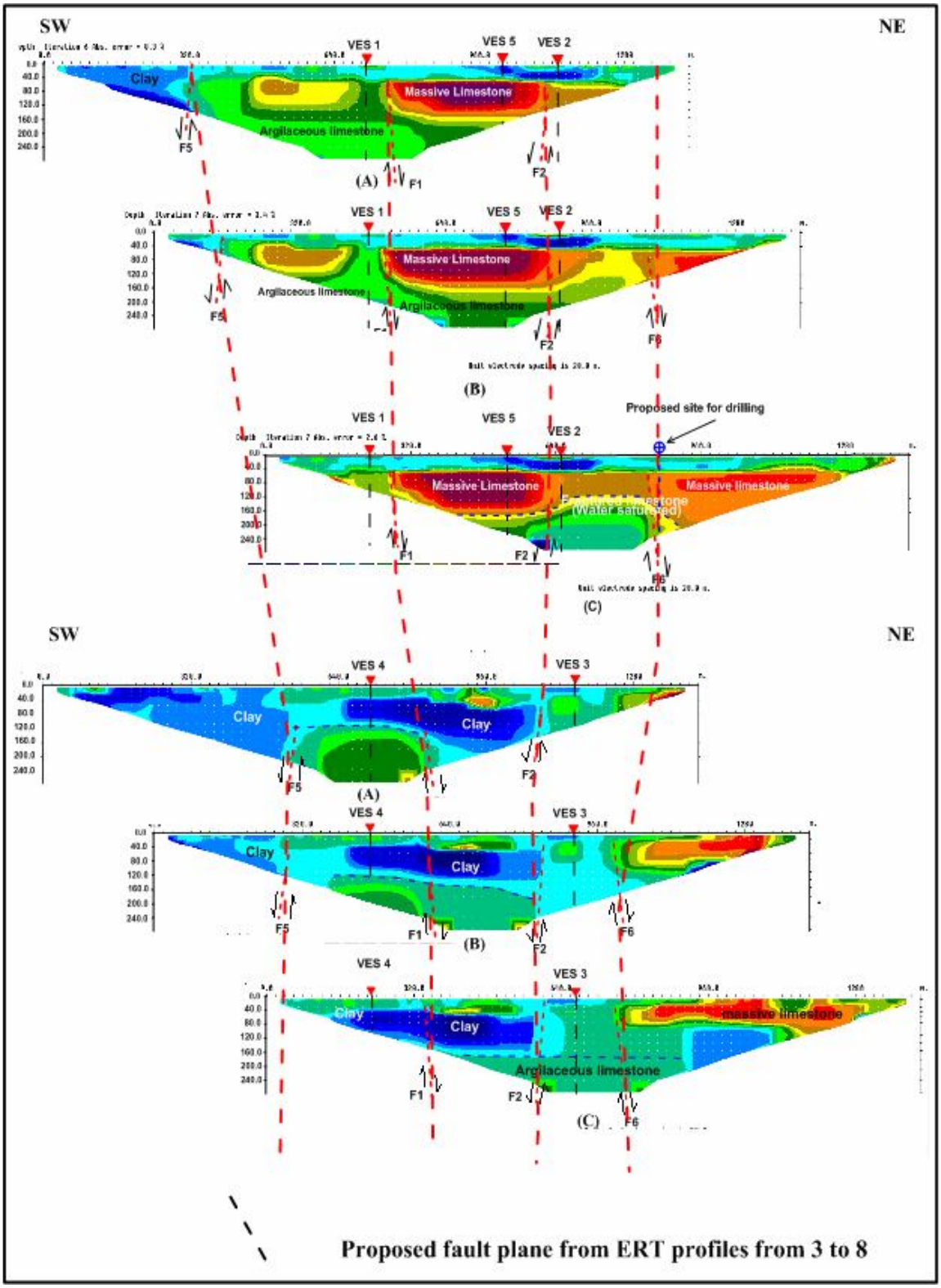

Fig. (12): The Inferred fault planes along the two summits inverted 2D sections.

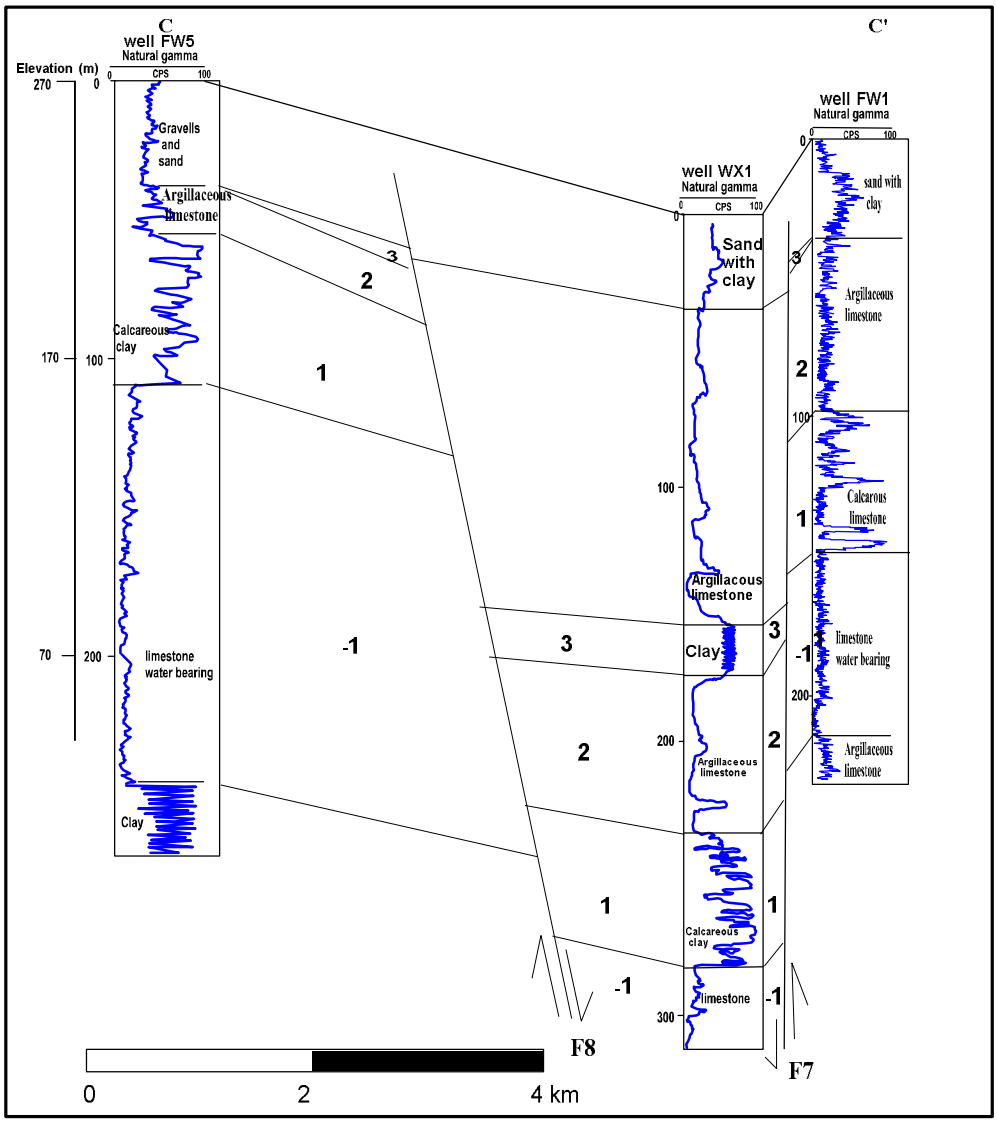

Fig. (13): Natural gamma and lithological logs correlation along profile C-C'.

Table (2): Hydrogeological of Wadi El Khariq wells.

Well No.	Aquifer	Total depth (m)	Depth to water m)	Hydraulic parameters
FW1	Upper Jurassic Massagid Formation (L.S)	215	101	Transmisivity (T) values vary from 6X10-5 to 2 X 10-2 m2/sec. The storativity (S) values vary from 4.3X10-1 to 5X10-3. The discharge value (Q) varies from 60 m3/h to 12 m3/h.
DRC2		338	100	
FW5		315	98	
FW2		200	106	
WX1		315	60	
DRC1		320	114	

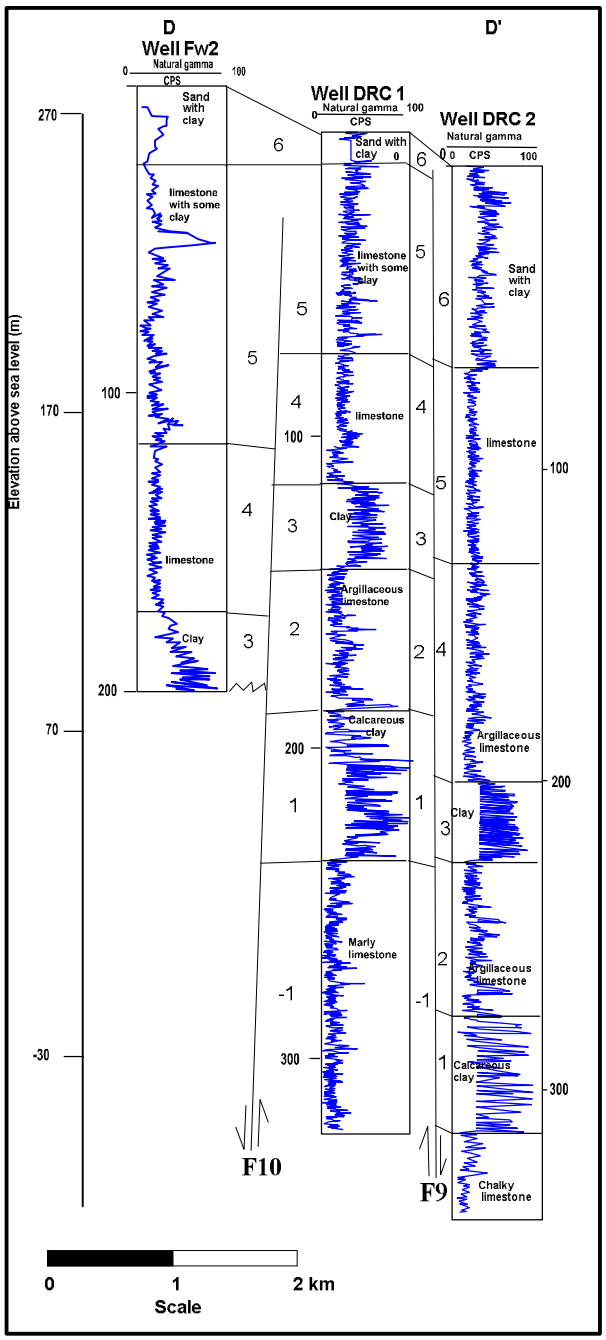

Fig. (14): Natural gamma and lithological logs correlation along profile D-D'.

The faults F7 and F8 form a graben in between so, the water bearing fractured limestone layer at the two limbs of the graben is found at a greater depth in the graben. On the other hand, the faults F9 and F10 form a horst structure between them. These structures play an immense role in facies changes laterally and variation in layers thickness. The fault F5 detected from the 2DERT coincides with the fault F7 that detected from gamma ray correlation in the trend and throw. Therefore, these two faults may be the same fault. The lineation analyses for the faults and fracture systems affected on Wadi El Khariq plain from the geological map (Fig. 3) is shown in figure 17 A. The main fracture azimuths are N 40 -50 W with L% 26.83 and N% 28.07, followed by N 50 -60 W with L% 16.78 and N% 15.79, and followed by N 30-40 E with L% 11.35 and N% 8.78. The fracture azimuths of the faults detected from the 2D imaging profiles of the geoelectrical field measurements (Fig. 17 B) are N 50 -60 W with L% 34.38 and N% 33.33, followed by N 70 -80 W with L% 32.09 and N% 33.33, and followed by N 0 - 10 E with L% 16.04 and N% 16.66. Also fracture azimuths of the faults detected from gamma log correlation and the constructed hydrogeological cross sections (Fig. 17 C) are N 40 -50 W with N% 33.33, followed by N 20 -30 W with N% 16.17, N 70 -80 W with N% 16.17, N 80 -90 W with N% 16.17and N 20 -30 E with N% 16.17. Therefore, the main fracture azimuths of the geological map nearly have the same azimuths of the faults detected from both the 2D imaging profiles and the gamma log correlation as well as the constructed hydrogeological cross sections.

CONCLUSIONS AND RECOMMENDATION

The interpretation of the Vertical Electrical Soundings revealed that the Water-bearing formation in the study area is represented by the fractured limestone (the third geoelectrical layer) and the argillaceous limestone (the fourth geoelectrical layer). The water bearing fractured limestone layer was not detected at some VESes due to the effect of structures and the lateral changes. Two normal faults (F1 and F2) are detected from the constructed geoelectrical cross sections. The interpretation results of the two Dimension geoelectrical resistivity tomography show that the area of study is characterized by heterogeneity for resistivity values in vertical and horizontal direction due to the effect of structural faults in the study area. The faults F1 and F2 were confirmed with that detected from VES. The 2D ERT profiles revealed that the clay content increase at the eastern part of the study area (2D numbers P6, P7 and P8). Therefore, the argillaceous limestone water-bearing is characterized by high salinity. On the other hand, the fractured limestone of moderate resistivity values (> 55-100 Ohm-m) and the argillaceous limestone (21-55 Ohm-m) represent the water-bearing layers at the other 2DERT profiles. In addition to F1 and F2 four other faults (F3-F6) were detected. The correlation results of the natural gamma and lithological logs of the drilled wells as well as the constructed hydrogeological cross sections revealed that the area of study affected by another group of faults (F6-F12). These faults have impact on the groundwater occurrence and quality of groundwater as these structures lead to lateral facies changes and variation in layers thickness. These fractures lead to the formation of graben and horst structures and these cause the fractured limestone layer lying beneath the calcareous clay is found at variable depths in the study area due to the impact of faults affecting the study area.

Most of the detected faults in the study area have NW-SE trends. This trend coincides with the lineation analyses for the faults and fracture systems affected on Wadi El Khariq plain.

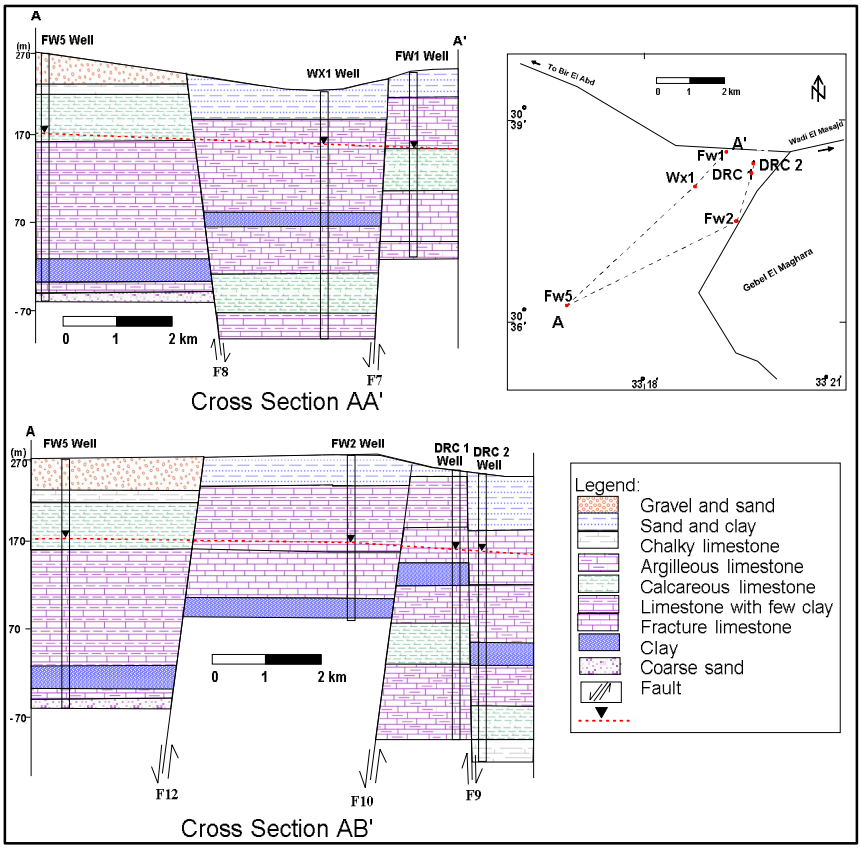

Fig. (15): Hydrogeological cross sections of Wadi El Khariq plain.

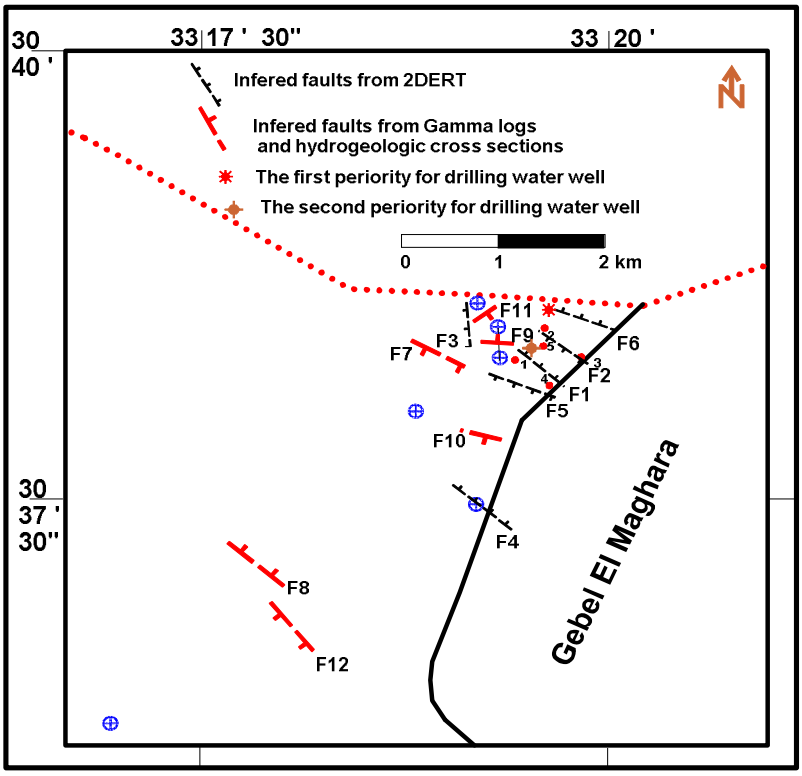

Fig. (16): Inferred structure from electrical studies, Natural gamma and lithological logs correlation and hydrogeological cross sections.

The fractured limestone in the study area is recharged by the percolation of the surface runoff water of local precipitation on Gable El Maghara catchment area through the fracture lines, fault planes and bedding planes besides paleowater of the paleo-rainy seasons. The groundwater salinity of the drilled wells in El Khariq plain varies from 2335 mg/l to 12548 mg/l. The discharge value (Q) varies from 60 m^3/h to 12 m^3/h. This variation is related to the extension and type of the effective fracture system affecting the concerned water bearing.

Although the 1D (VES) give information about resistivity and structure in both vertical and horizontal directions the 2D profiles give more precise details about the vertical and horizontal variations in resistivity values, vertical and horizontal lithological facies changes, the depth to water and the exact structures locations, it is recommended to use 2D ERT technique in dealing with karast aquifer.

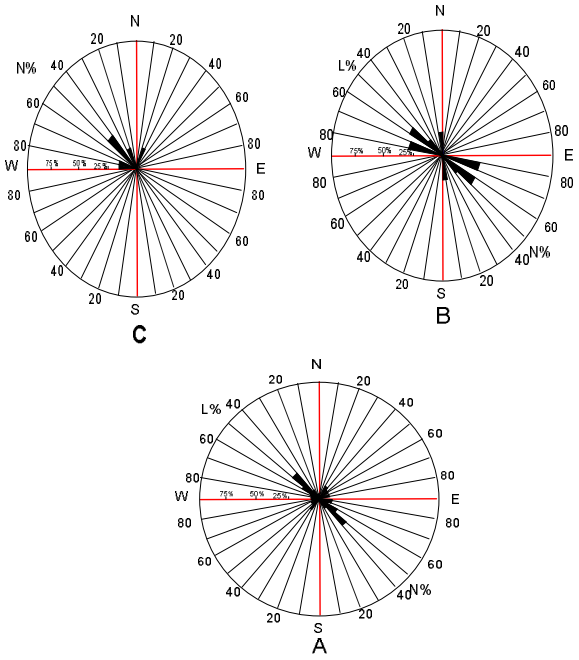

Fig. (17): Rose diagram of faults and fractures of Wadi El Khariq plain.

REFERENCES

Al-Far, D.A. (1966): Geology and Coal Deposits of Gebel El Maghara, Northern Sinai. Geol. Surv. Egypt. 59 p.

Alile, O.M., Ujuanbi, O., Evbuomwan, I.A. (2011). Geoelectric investigation of groundwater in Obaretin -Iyanomon locality, Edo state, Nigeria. J. G. Mining Res., 3(1): 13-20.

Barker, R.D., (1996): The application of electrical tomography in groundwatercontamination studies. EAGE 58th Conference and TechnicalExhibition Extended Abstracts, P082.

Butzer, K.W. (1960): Environment and human ecology in Egypt during Pre-Dynastic and early Dynastic Times. Bull. Soc. Geogr. Egypt, 32; 42-88.

Chalikakis, K.V., Plagnes, R., Guerin, R. Valois and F.P. Bosch (2011): Contribution of geophysical methods to karst-system exploration: An overview, Hydrogeol. J., 19, 1169–1180, doi:10.1007/s10040-011-0746-x.

Dobrin, M.B. (1988). Introduction to Geophysical Prospecting. New York: McGraw-Hill, p. 867.

Dunscomb, M. and E. Rehwold, (1999): Two-dimensional resistivity profiling; geophysical weapon of choice in karst terrain for engineering applications, in Seventh Multidisciplinary Conference on Sinkholes and the Engineering and Environmental Impacts of Karst, Harrisburg-Hershey, PA, p. 478.

Egyptian Geological Survey and Mining Authority (EGSMA, 1985): Hydrogeological Testes at the Exploratory Water well WX-2 El Maghara Coalfield.

Egyptian Geological Survey and Mining Authority (EGSMA, 1986): Hydrogeological Investigations at El Maghara Area; Progressive Report No.4 (September).

EI Ghazawi, M.M. (1989): Hrogeological studies in Northeast Sinai, Egypt. Thesis submitted for the Degree of Ph. D. Fac. of Sci. Mansoura Uni. 290 p.

EL Ghazawy, M.M. (1999): "A simulation model for groundwater exploration in fractured carbonate aquifers in El Maghara, north Sinai, Egypt", J. Environ Sci. Vol. 18, pp. 47-60.

El Abd, E.A. (2000): Contribution to the hydrogeology of Northwest Sinai, Egypt. M. Sc. Thesis, Fac. Sci., Minufiya Univ., Egypt, 165p.

El Abd, E.A. and Sadek, A.A. (2010): Geochemistry of Middle and Upper Jurassic water bearing formations in Gabal El Maghara, Northwest Sinai, Egypt. Bull. Soc. Sedimentology of Egypt, vo.l 18, p. 147-160

Ford, D.C. and P. Williams (2007): Karst Hydrogeology and Geomorphology, John Wiley, Chichester, U. K.

Foster Wheeler Italian-Fosweco Division (1990): Gebel El Maghara Rural Development Project Final Report, Submitted to the Governorate of North Sinai, Five Volumes.

Geofizika Co. (1963): Report on Investigation of Water and Soil Resources in the North and Central Part of Sinai Peninsula, Report Submitted to General Desert Development Authority, pp. 186.

Geological Survey of Egypt (G.S.E.) (1992-1994): Geologic Maps of Sinai. Scale 1:250,000 Sheets 3 and 5. Geol. Surv.Egypt, Cairo, Egypt.

Griffiths, D.H. and Barker, R.D. (1993) Two-dimensional resistivity imaging and modeling in areas of complex geology. Jour. of Applied Geoph., 29, Elsevier Science Publishers, B.V., Amsterdam, pp. 211-226.

Hammad, F.A. (1980): Geomorphological and Hydrogeological Aspects of Sinai Peninsula. 5th Africa conference, A.R.E., Ann. Geol. Surv. Egypt, Vol. 10, pp. 807-817.

Hassanein, A.M. (1997): Geological and Geomorphological Impacts on the Water Resources in the Central Sinai, Egypt. Ph. D. Thesis, Fac. Sci. Ain. Shams. Univ. 373 p.

Japan International Cooperation Agency (Jica) (1992): North Sinai Groundwater Resources study in the Arab Republic of Egypt. Final Report Submitted to the Research Institute For Water Resources Ministry of Public Works and Water Resources, Cairo, Egypt, 207p.

***Jardani, A., A. Revil, F. Santos, C. Fauchard and J. P. Dupont (2007):** Detection of referential infiltration pathways in sinkholes using joint inversion of self-potential and EM-34 conductivity data, Geophys. Prospect., 55, 749–760, doi:10.1111/j.1365-2478.2007.00638.x.

IPI2win program (2003): Resistivity Sounding Interpretation program Version 3.0.1.a 7.01.03(2003). Moscow State University, Moscow

Kumar, D., Ahmed, S., Krishnamurthy, N.S., Dewandel, B. (2007). Reducing ambiguities in vertical electrical sounding interpretations: A geostatistical application. J. A. Geophys., 62: 16-32.

Legchenko, A., M. Ezersky, C. Camerlynck, A. Al-Zoubi, K. Chalikakis, and J. F. Girard (2008): Locating water-filled karst caverns and estimating their volume using magnetic resonance soundings, Geophysics, 73(5),G51–G61, doi:10.1190/1.2958007.

Loke, M.H. (1998): "RES2DINV" V. 3.4, rapid 2D resistivity inversion using the least square method. ABEM instrument AB, Bromma,Sweden

Loke, M.H. (1999): Electrical imaging surveys for environmental and engineering studies. Apractical guide to 2D and 3D surveys: Austin, Texas, Advanced Geosciences Inc., p. 57.

Loke, M.H. (2001): Electrical imaging surveys for environmental and engineering studies: a practical guide to 2D and 3D surveys, 62 pp.

Mahmoud, H.H., Barseem, M.S.M., Youssef, A.M.A. (2015): Application of the two dimensional geoelectric imaging technique to explore shallow groundwater in Wadi El Gerafi basin, Eastern Central Sinai – Egypt.Arab. J. Geosci., 8, 3589-3601, DOI 10.1007/s12517-014-1498-4

Marescot, L., Loke, M.H. (2003): Using the depth of investigation indexmethod in 2D resistivity imaging for civil engineering surveys.SAGEEP 2003. Denver, USA.

McGrath, R.J., P. Styles, E. Thomas and S. Neale (2002): Integrated high resolution geophysical investigations as potential tools for water resource investigations in karst terrain, Enivron. Geol., 42, 552–557, doi:10.1007/ s00254-001-0519-2.

Olayinka, A.I., Yaramanci, U., (2000): Use of block inversion in the 2-Dinterpretation of apparent resistivity data and its comparison withsmooth inversion. J. Appl.Geophys., 45, 63–82.

Osella, A., Favetto, A., Martinelli, P., Cernadas, D., (1999): Electrical imaging of analluvial aquifer at the Antinaco-Los Colorados tectonic valley inthe Sierras Pampeanas, Argentina. J. Appl. Geophys., 41, 359–368

Ozcep, F., Tezel, O., Asci, M. (2009): Correlation between electrical resistivity and soil-water content: Istanbul and Golcuk. Int. J. Phys. Sci., (4)6: 362-365

Research Institute For water Resources (RIWR) (1984): Well Technical Report PW and PZ No. 12; Wadi El Khariq; El Maghara Area. Internal Report El-Kanater El-Khyria. WRC. Egypt.

Research Institute For water Resources (RIWR) (1988): The Water balance for Groundwater In north Sinai, April 1988. Internal Report El Kanater El - Khyria. WRC. Egypt.

Schoor, V. M., (2002): Detection of sinkholes using 2D electrical resistivity imaging. J. Appl.Geophys., 50, 393–399

Shata, A. (1956): Structural Development of the Sinai Peninsula, Egypt, Bull. Inst. Desert, Egypt, 6(2), pp. 117-157.

Sumanovac, F., and M. Weisser (2001): Evaluation of resistivity and seismic methods for hydrogeological mapping in karst terrains, J. Appl.Geophys., 47, 13–28, doi:10.1016/S0926-9851(01)00044-1.

Sumanovac, F. (2006): Erratum toMapping of thin sandy aquifers by usinghigh resolution reflection seismics and 2-D electrical tomography. J. Appl.Geophys., 59, 345–346.

Thomas, B., and M.J.S. Roth (1999): Evaluation of site characterization methods for sinkholes in Pennsylvania and New Jersey, Eng. Geol. Amsterdam, 52, 147–152, doi:10.1016/S0013-7952(98)00068-4.

Yehia, M.M. (1994): Hydrogeological and Hydrochemical studies of the deep aquifers in some localities in Sinai Peninsula. Ph. D. Fac. of Sci. Menofia Univ. 327p.

Yilmaz, S. (2011). A case study of the application of electrical resistivity imaging for investigation of a landslide along highway. Int. J. Phys. Sci., 6(24): 5843-5849. Zaidi KF,

Van Schoor, M. (2002): Detection of sinkholes using 2D electrical resistivity imaging, J. Appl. Geophys., 50, 393–399, doi:10.1016/S0926-9851(02) 00166-0.

Van Der Velpen, B. P. A., (1988): "RESIST", version 1.0, a package for the processing of the esistivity sounding data, M. Sc. Research Project, ITC, Deft, the Netherlands.